Philosophical Magazine
Vol. 89, Nos. 22–24, 1–21 August 2009, 1933–1946

Taylor & Francis
Taylor & Francis Group

Domain walls and domain wall resistivities in $Co_xPd_{1-x}(111)$ and $Co_xPt_{1-x}(111)$

P. Weinberger*

Center for Computational Nanoscience, Seilerstätte 10/22, A-1010 Vienna, Austria

(*Received 19 November 2008; final version received 16 December 2008*)

In using the relativistic screened Korringa–Kohn–Rostoker method and a multi-scale approach based on a parametrization of the Ginzburg–Landau expansion of the free energy as a functional of the magnetization density, domain wall widths in Co_xPd_{1-x} and Co_xPt_{1-x} are determined by considering these substitutionally disordered alloys as two-dimensionally invariant systems. It is shown that in Co_xPd_{1-x}, domains are formed nearly over the whole concentration range, while in Co_xPt_{1-x}, domain wall formation only occurs near 50% Co and for Co-rich alloys. Based on these results resistivities in the presence and absence of domains walls are evaluated in terms of the relativistic Kubo–Greenwood equation. In contrast to Co_xNi_{1-x}, it turns out that both systems are unsuitable as race track materials.

Keywords: magnetic structure; magnetic alloys; electrical transport; magneto-resistance

1. Introduction

The (bulk) phase diagram of Co_xPd_{1-x} [1] shows no ordered phases: Co and Pd form a continuous series of fcc solid solutions with complete solubility at all compositions. The phase diagram of Co_xPt_{1-x} [1] on the other hand exhibits two superstructures, namely at $x = 0.25$ and 0.5, but otherwise seems to be statistically disordered on an fcc lattice. Co/Pd and Co/Pt are well-studied systems in the literature with available investigations ranging from typical bulk studies [2–5], free surfaces of Co on Pd and Pt [6], (phenomenological) micromagnetic studies of magnetization switching [7–10], *ab initio* attempts thereof [11], small Co clusters or nanostructures on top of Pt [12–14], *ab initio* descriptions of magneto-optical properties [15,16], to attempts to measure and characterize domain wall resistivities [17].

Studies of domain walls in nanowires and their resistivities suddenly became very prominent once the idea of race track memories was coined, namely the suggestion to use current driven domain wall motions as an underlying physical principle for a completely new type of solid state memory device [18–23]. This idea started a series of theoretical investigations dealing with exactly the set-up used in the experimental studies [24–27], partially performed in the hope of suggesting other systems [26,27]

*Email: weinberger@computational-nanoscience.de

ISSN 1478–6435 print/ISSN 1478–6443 online

DOI: 10.1080/14786430802698894
http://www.informaworld.com

than permalloy [24,25]. In this context also the present paper has to be seen, namely as an attempt to learn more about domain wall formation in Co_xPd_{1-x} and Co_xPt_{1-x} and to find out whether at least one of these systems could serve as a race track material.

2. Formal concepts and computational details

2.1. *Magnetic configurations and domain wall formation energies*

In principle, the orientations of the magnetization in an infinite layered system characterized by two-dimensional translational invariance (one atom per unit cell), see Figure 1, are defined by the following set of unit vectors

$$C = \{\vec{n}_l, \vec{n}_1, \vec{n}_2, \ldots, \vec{n}_i, \ldots, \vec{n}_L, \vec{n}_r\}, \tag{1}$$

where $\vec{n}_l$ refers to the uniform direction of the magnetization in the left domain (semi-infinite system), $\vec{n}_r$ to that in the right domain (semi-infinite system) and the $\vec{n}_i$ to those in the L atomic layers forming the domain wall. Equation (1) specifies a typical non-collinear magnetic configuration in a layered system corresponding to a simple parent lattice. There are two special cases, namely C_0,

$$C_0 : \vec{n}_l = \vec{n}_r = \vec{n}_i = \vec{z}, \quad i = 1, L, \tag{2}$$

in which the magnetization in all atomic layers of the system points along the surface normal ($\vec{z}$), and C_1,

$$C_1 : \vec{n}_l = \vec{n}_r = \vec{n}_i = \vec{x}, \quad i = 1, L, \tag{3}$$

referring to a uniform orientation of the magnetization along the in-plane $\vec{x}$ axis. C_0 and C_1 are of course so-called collinear magnetic configurations. In principle, in the domain wall, the $\vec{n}_i$ can vary in an arbitrary manner implying that for a given L the total energy of the whole system has to be minimized with respect to all possible non-

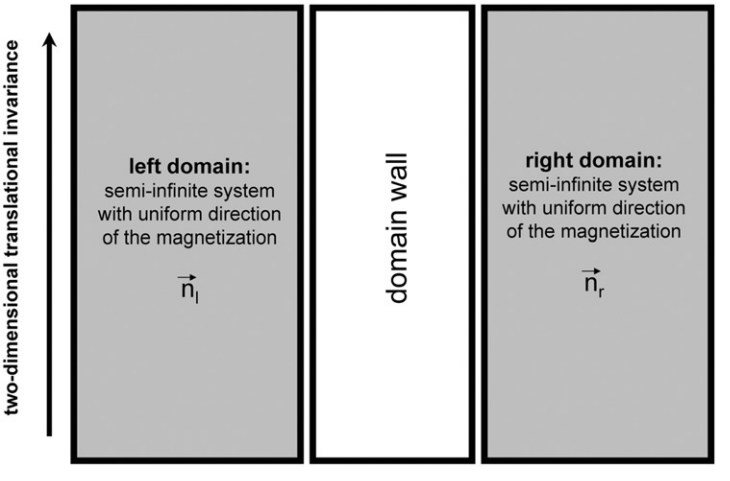

Figure 1. Schematic view of a 180° domain wall.

collinear arrangements in the domain wall in order to determine the most favorable configuration. Since such a procedure is usually computationally not feasible, a model for the orientations in the various atomic layers in the domain wall is adopted. Here the following scheme for a 180° domain wall is applied:

$$C_d : \vec{n}_l = \vec{z}, \quad \vec{n}_r = -\vec{z}, \quad \vec{n}_i = \mathbb{D}(\Phi_i)\vec{y}, \qquad (4)$$
$$\Phi_i = 180i/L, \quad i = 1, L,$$

which describes a quasi-continuous change of the orientation of the magnetization from $\vec{z}$ to $-\vec{z}$. In Equation (4), $\mathbb{D}(\Phi_i)$ is the three-dimensional representative of a rotation around the $\vec{y}$ axis (perpendicular to $\vec{x}$ and $\vec{z}$) by an angle Φ_i.

In using the so-called magnetic force theorem the domain wall formation energy at a given value of L is then defined by the difference in the grand potentials between configurations C_d and C_0,

$$E(L, x) = E(L, x, C_d) - E(L, x, C_0) \qquad (5)$$
$$= \sum_{p=1}^{N} (E^p(L, x, C_d) - E^p(L, x, C_0)), \qquad (6)$$

where x is the concentration, p denotes atomic layers, and N includes a sufficient number m of 'buffer' atomic layers in the left and right domain in order to guarantee a smooth transition between the domain wall and its adjacent domains,

$$N = L + 2m. \qquad (7)$$

The layer-resolved contributions $E^p(L, x, C_i)$ to the grand potential are given by

$$E^p(L, x, C_i) = \int_{E_b}^{E_F} n^p(L, x, C_i, z)(z - E_F)\mathrm{d}z, \qquad (8)$$

where $n^p(L, x, C_i, z)$ is the density-of-states of the p-th atomic layer in a domain wall of width L corresponding to a magnetic configuration $C_i = C_0$, C_1 or C_d. In Equation (8), $z = \epsilon + i\delta$ is, in general, a complex energy, E_b the valence band bottom and E_F the Fermi energy. It should be noted that Equation (5) implies that for $E(L, x) > 0$ configuration C_d (domain wall formation) is preferred, while for $E(L, x) \leq 0$ configuration C_0 is the stable one (the system forms a single domain with the direction of the magnetization pointing uniformly along $\vec{z}$).

Since the minimum in $E(L, x)$ with respect to L,

$$\left.\frac{\mathrm{d}E(L, x)}{\mathrm{d}L}\right|_{L_0} = 0, \qquad (9)$$

usually occurs at rather large values of L, it was suggested [28] casting the Ginzburg–Landau expansion of the (generalized) free energy as a functional of the magnetization density into a multi-scale approach, since then the $E(L, x)$ can be formulated in terms of two constants $a(x)$ and $b(x)$,

$$E(L, x) = A(x)\left(\frac{a(x)}{L} + b(x)L\right), \qquad (10)$$

the first one being the so-called exchange, the second one the anisotropy energy parameter. The equilibrium width of the domain wall for a given concentration x is then simply given by

$$L_0(x) = +\sqrt{a(x)/b(x)}. \tag{11}$$

It should be noted that since $E(L, x)$ is quadratic in L, in principle the value of $E(L, x)$ needs to be determined only at two (large enough) values of L in order to evaluate $L_0(x)$. The above described multi-scale approach was rigorously tested [28] and successfully applied to permalloy [24,26,27] and Co_xFe_{1-x} and Co_xNi_{1-x} [25].

2.2. *Sheet resistances and resistivities*

In principle, for a particular magnetic configuration C_i the current perpendicular to the planes of atoms (CPP) defined over a certain length L is given by (see, for example, [29])

$$\rho_{\mathrm{CPP}}(L, x, C_i) = \frac{1}{L} \iint_{-\infty}^{\infty} \rho(z, z'; x, C_i) \mathrm{d}z \, \mathrm{d}z', \tag{12}$$

and the corresponding sheet resistance by

$$r(L, x, C_i) = L\rho_{\mathrm{CPP}}(L, x, C_i). \tag{13}$$

For large enough L the resistivity $\rho_{\mathrm{CPP}}(L, x, C_i)$ can be obtained from the zz-component of the conductivity tensor, $\sigma_{zz}(L, x, C_i)$,

$$\rho_{\mathrm{CPP}}(L, x, C_i) \sim \rho_{zz}(L, x, C_i) = \sigma_{zz}^{-1}(L, x, C_i). \tag{14}$$

As it is virtually impossible to calculate the conductivity tensor by means of *ab initio* methods for very large L one can make use of the fact that $r(L, x, C_i)$ is linear in L,

$$r(L, x, C_i) = L\rho_{zz}(L, x, C_i) = \alpha(x, C_i) + \beta(x, C_i)L, \tag{15}$$

which, furthermore, has the useful limiting properties

$$0 < x < 1 : \lim_{L\to\infty} \rho_{zz}(L, x, C_d) = \beta(x, C_d) = \rho_{zz}(x, C_0), \tag{16}$$

$$x = 0, 1 : \lim_{L\to\infty} \rho_{zz}(L, x, C_d) = \rho_{zz}(C_0) = 0. \tag{17}$$

In Equation (16), $\rho_{zz}(x, C_0)$, $0 < x < 1$, is the zz-component of the residual ('bulk') resistivity corresponding to configuration C_0 (see Equation (2)). As is well-known for pure systems ($c = 0, 1$) the constant $\beta(C, c)$ has to be exactly zero. Equation (17) can therefore be used to check the accuracy of the applied numerical procedure, in particular, since $\rho_{zz}(L, x, C_i)$ is evaluated by means of an analytical continuation of resistivities defined for complex Fermi energies; for a review see [30].

3. Numerical details

All *ab initio* calculations for $Co_xPd_{1-x}(111)$ and $Co_xPt_{1-x}(111)$ were performed at the experimental lattice constant using Vegard's law, e.g.

$$a_0(x) = xa_0(Co) + (1-x)a_0(Pd),$$

(Co: 6.5509, Pd: 7.3530, Pt: 7.4137 [a.u.]) in terms of the spin-polarized (fully) relativistic screened Korringa–Kohn–Rostoker (SPR-KKR) method within the framework of the inhomogeneous Coherent Potential Approximation [31]. It should be noted that Vegard's law describes the variation of the experimental lattice parameter of Co_xPd_{1-x} and Co_xPt_{1-x} with respect to the concentration rather well [1].

In using the self-consistent potentials and exchange fields corresponding to configuration C_0, the grand potentials $E(L, x)$, see Equation (5), were evaluated by means of a contour integration along a semicircle using a 16-point Gaussian quadrature and 1830 k points per irreducible part of the surface Brillouin zone (ISBZ). The equilibrium domain wall width was then determined at $L = 222$ and 324 [ML]. For an extensive discussion of the accuracy of the fit based on Equation (10) using the same numerical parameters see [24].

The electric transport properties were evaluated at complex Fermi energies by means of the fully relativistic Kubo–Greenwood equation (for a review see [30]) also using 1830 k points per ISBZ and then analytically continued to the real axis. All resistivities at L_0 and $L = \infty$ (bulk) were determined via Equation (15) using the calculated values of $r(L, x, C_i)$ at $L = 60$ and 120 [ML]. A detailed study of the numerical properties of Equation (15) is to be found in [32], in which not only the L dependence is discussed but also the accuracy of the analytical continuation to the real axis. It should be noted that for both fits, namely employing Equations (10) and (15), sufficiently large values of L, well separated from each other, were used in order to exclude any kind of 'neighborhood effects'. For computational reasons, the two values had to be smaller in the case of the electric properties. However, in principle – as was already mentioned and was amply discussed in [24,32] – for these fits an arbitrary pair of values of L can be chosen. In both types of calculations the number of 'buffer layers', see Equation (7), was three.

Since a (111) stacking sequence was chosen for both systems, the equilibrium domain wall width in [nm] and the unit area in $[\text{nm}]^2$ is defined by

$$L_0[\text{nm}] = \frac{a_0(x)}{\sqrt{3}} L, \quad A(x)[\text{nm}]^2 = \frac{\sqrt{3}a_0^2(x)}{4},$$

where L is the number of atomic layers at which Equation (9) is fulfilled.

4. Discussion of results

4.1. *Spin and orbital moments*

As already stated in the introduction, the bulk systems Co_xPd_{1-x} and Co_xPt_{1-x} are well-studied in the literature, and yet surprising features are found when they are directly compared to each other. In Figure 2 the spin and orbital moments of Co and

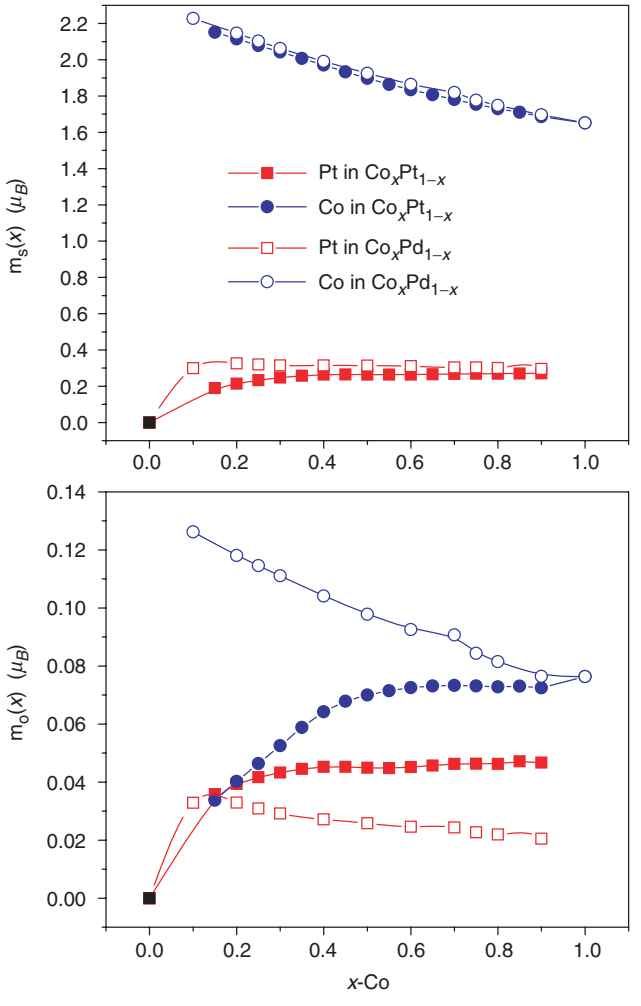

Figure 2. Spin and orbital moments in fcc $Co_xPd_{1-x}(111)$ and fcc $Co_xPt_{1-x}(111)$.

Pd (Pt) are shown versus the concentration x. As can be seen the spin moments in the two substitutionally disordered systems are very much alike. There are hardly any differences in the Co spin moment whether Co is alloyed with Pd or Pt. Also, the induced spin moments for Pd and Pt are very similar in value through the whole studied concentration range. However, the orbital moments behave completely differently: with decreasing Co content in Co_xPd_{1-x} the Co orbital moments increase substantially while in Co_xPt_{1-x} they decrease. Taking for example the values at $x = 0.25$ the difference is about 0.07 [μ_B]. This *per se* is quite a big value for an orbital moment! Also, the induced orbital moments at Pd or Pt sites are remarkably different. For large Co concentrations they differ by nearly a factor of 2.

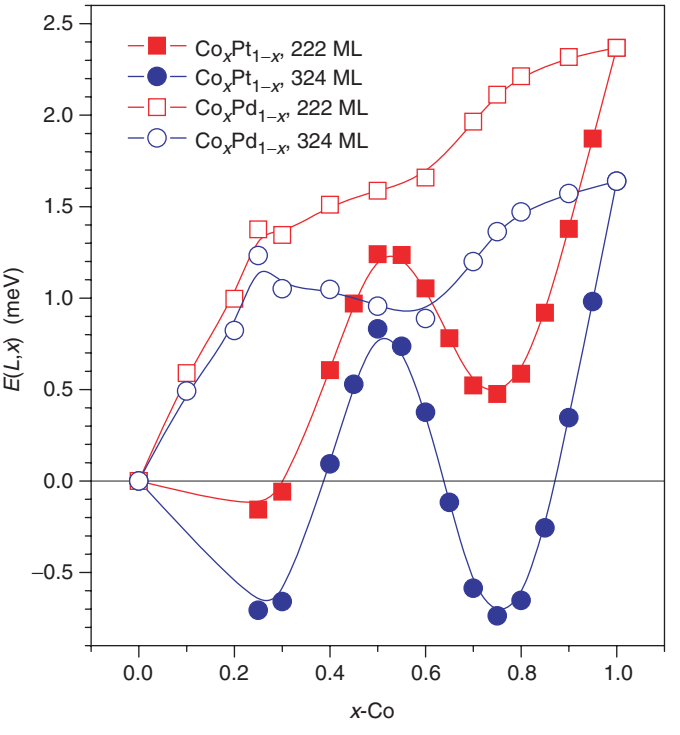

Figure 3. Domain wall formation energies in fcc $Co_xPd_{1-x}(111)$ and fcc $Co_xPt_{1-x}(111)$.

4.2. *Domain wall formation energies and domain wall widths*

Turning now to the domain wall formation energies, see Equation (5), displayed in Figure 3 for $L = 222$ and $L = 324$, it seems that two completely different systems are dealt with, in particular since in the case of Co_xPt_{1-x} the domain wall energy for $L = 324$ is negative for $x < 0.4$ and $0.6 < x < 0.9$. From Equation (5) – as should be recalled – it follows directly that in these concentration ranges the magnetic configuration C_0 is preferred, i.e. the magnetization is uniformly aligned in all atomic layers of the system along the surface normal. This of course implies that no domains and therefore domain walls are formed.

It is interesting to explore from which parts in a domain wall of given width the main contributions to the domain wall formation energy arise. In order to illustrate corresponding changes with respect to the concentration in Figure 4 the layer-resolved quantities, see Equations (5) and (6), are displayed for $L = 324$ and $x = 0.1$, 0.3 and 0.5 in the case of Co_xPd_{1-x}. Quite obviously these layer-resolved domain wall energies vary rapidly at the very beginning and end of the domain wall. In the lower part of this figure, this particular feature is shown for the first 10 atomic layers. As can be seen, the rise to a certain value occurs within the first five layers.

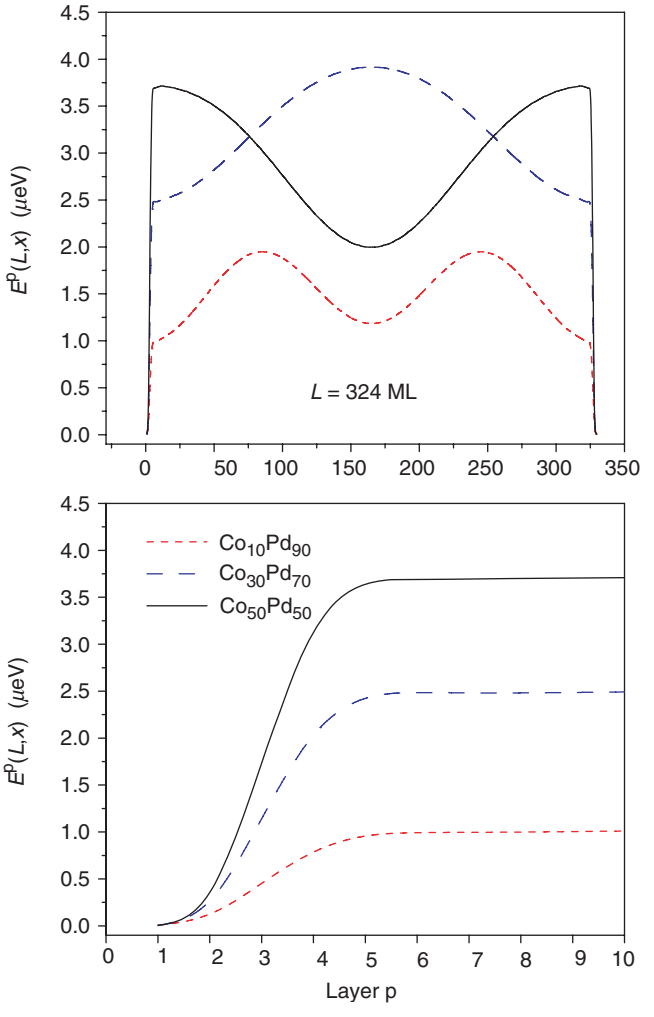

Figure 4. Layer-resolved domain wall formation energies in fcc $Co_xPd_{1-x}(111)$.

In the interior of a domain wall, the layer-resolved domain wall formation energies vary differently for different concentrations. For example, at $x = 0.5$ there is a minimum in the middle of the domain wall, while for $x = 0.3$ a maximum is present. In the middle of a domain wall the orientation of the magnetization is perpendicular to that in the adjacent domains, indicating a higher ($Co_{30}Pd_{70}$) or lower ($Co_{50}Pd_{50}$) contribution to the in-plane anisotropy of the respective atomic layers. In the case of $Co_{10}Pd_{90}$, there are even two maxima, which occur separated symmetrically by a minimum in the middle of the wall. From Figure 4 it follows that obviously the 'interface' of the domain wall with its adjacent domains is of crucial importance, a fact that most likely will have to enter an *ab initio* description of domain wall motions. In Figure 5 for $Co_{50}Pd_{50}$, $L = 324$, the contributions of the components Co and Pd to the domain wall formation energy are depicted. As can be seen, the

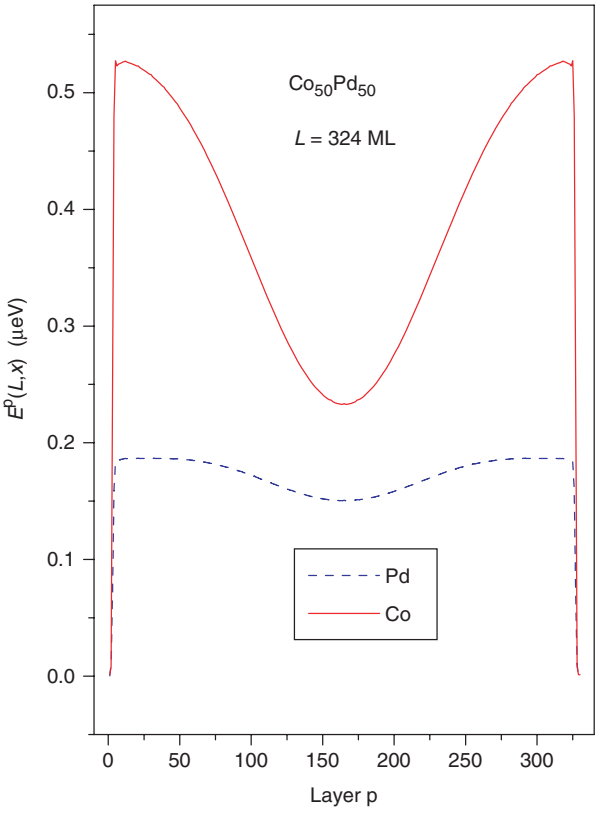

Figure 5. Component and layer-resolved domain wall formation energies in fcc $Co_{50}Pd_{50}(111)$.

contribution from Pd is surprisingly large in particular in the middle of the domain wall.

To illustrate the variation of $E(x, L)$ with L, in Figure 6 a few characteristic cases are shown for Co_xPd_{1-x}. It should be noted that in this figure, L is deliberately given in units of [ML] in order to prove the usefulness of Equation (10). From this figure it can be seen that for $x = 0.9$ the minimum is very shallow, while for $x = 0.1$ it is reasonably deep. In all cases, the actual equilibrium domain wall formation energy is rather small, namely less than about 50 [μeV]. The parameters for the fit, the exchange and the anisotropy energy, are displayed together with the equilibrium domain wall width in Figure 7. In particular from this figure the enormous differences between Co_xPd_{1-x} and Co_xPt_{1-x} become transparent; these were already present when discussing the orbital moments. With the exception of very dilute alloys of Co with Pd, over the whole concentration range in Co_xPd_{1-x}, 180° domains are formed. The width of these domain walls is surprisingly small for $x < 0.3$ and $0.5 < x < 0.7$. Because of the minimum in the anisotropy parameter at about $x = 0.4$, the domain wall width at this concentration becomes rather large, in the same manner as a decreasing anisotropy for high Co concentrations causes a steady

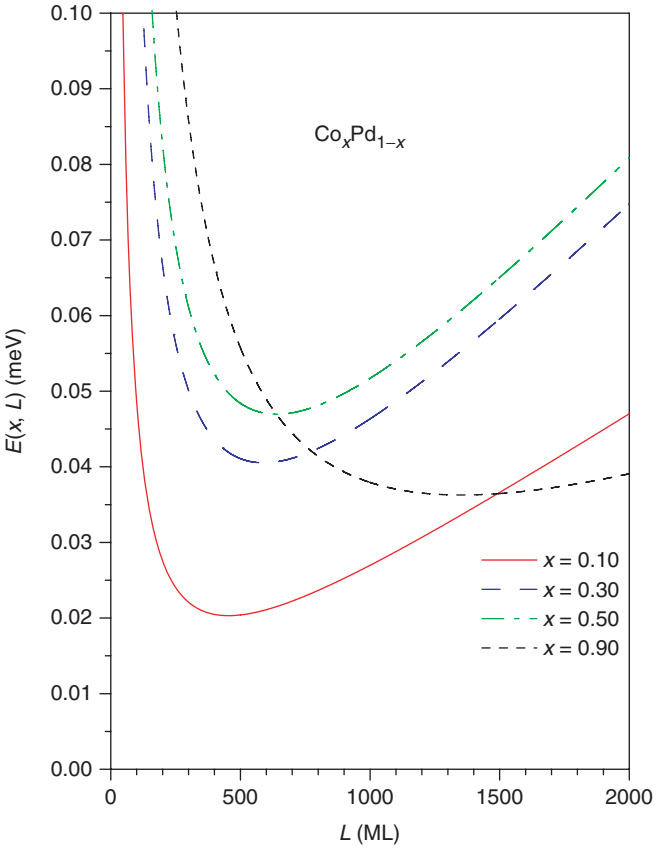

Figure 6. Fitted domain wall formation energies in fcc Co_xPd_{1-x}(111).

increase of the domain wall width. This behavior follows directly from Equation (11) since the anisotropy parameter serves as denominator.

For Co_xPt_{1-x}, the situation is completely different, since, as was already said, for $x < 0.4$ and $0.6 < x < 0.9$ the domain wall formation energies are negative causing the exchange parameter in Equation (11) to vanish. These are the concentration regimes in which no domain wall formation occurs. For $x > 0.9$, both the exchange as well as the anisotropy parameter vary rapidly. It seems that the anisotropy parameter is increasing in order to overcome the fast decline in the exchange parameter. Consequently, in this concentration regime, the equilibrium width changes very fast, with the concentration being very small indeed for $x = 0.9$.

4.3. *Domain wall resistivities*

Nowadays the main interest in domain walls is of course directed at their resistivities, in particular to the change in the anisotropic magnetoresistance (AMR) of

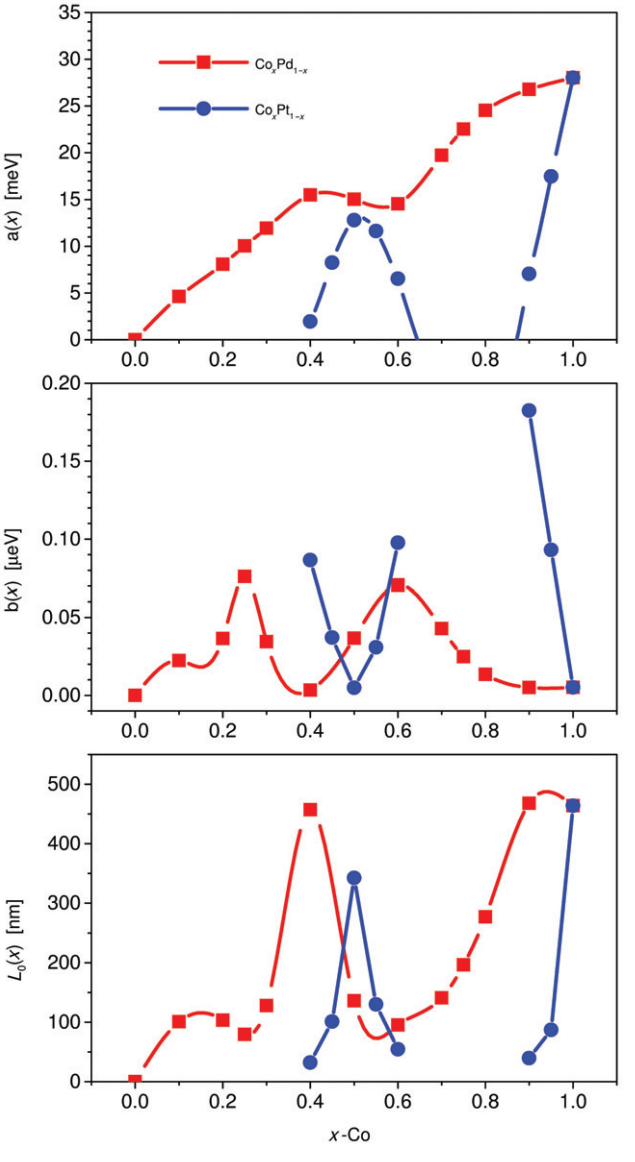

Figure 7. Exchange energy parameter (top), anisotropy parameter (middle) and equilibrium domain wall width in fcc $Co_xPd_{1-x}(111)$ and fcc $Co_xPt_{1-x}(111)$.

a statistically disordered system in the presence,

$$\mathrm{AMR}(L_0, x) = \frac{\rho_{zz}(L_0, x, C_d) - \rho_{zz}(L_0, x, C_1)}{\rho_{zz}(L_0, x, C_d)}, \tag{18}$$

and absence,

$$\mathrm{AMR}(x) = \frac{\rho_{zz}(x, C_0) - \rho_{zz}(x, C_1)}{\rho_{zz}(x, C_0)}, \tag{19}$$